Biophysical Chemistry 140 (2009) 122–128

Contents lists available at ScienceDirect

Biophysical Chemistry

journal homepage: http://www.elsevier.com/locate/biophyschem

Short communication

Multi-scale modelling of amyloid formation from unfolded proteins using a set of theory derived rate constants

Damien Hall *, Nami Hirota

Institute of Basic Medical Science, University of Tsukuba, Lab 225-B, Building D. 1-1-1 Tennodai, Tsukuba-shi, Ibaraki-ken, 305-8577, Japan

ARTICLE INFO

Article history:
Received 1 November 2008
Received in revised form 17 November 2008
Accepted 17 November 2008
Available online 6 December 2008

Keywords:
Amyloid
Structure
Kinetics
Mechanism
Distribution

ABSTRACT

Traditional simulation and analysis of amyloid aggregation kinetics has involved the examination of a single lumped parameter taken to reflect the total mass of protein in amyloid form. However use of increasingly sophisticated multi-experimental strategies capable of providing information on the structure of the growing fibril at the mesoscopic and atomistic level, has put extra information within the experimenter's reach. Although such data can be presented empirically, its incorporation into a theoretical model is more problematic due to scaling issues associated with modern day approaches which fall into either the particle based or statistical based categories. Here we present a coarse grained multi-scale simulation of irreversible amyloid formation that straddles this simulation divide by using a set of theory derived size and conformation specific rate constants to simulate the kinetic evolution of the amyloid fibril population. This approach represents a potentially profitable simulation/analytical strategy that will help to probe more deeply into the underlying molecular driving forces behind the phenomenon of amyloid formation.

Amyloid fibrils are β-sheet rich, long protein rod like structures, that are capable of being formed from the homo-polymerization of a variety of different proteins [1–6]. This diverse range of protein fibrils have caused much excitement over the last one hundred and fifty years due to their association with various diseases [7], their intrinsic biological function [8] and their potential use as a nanotechnology/material science agent [9]. Due to these relationships and also because of the fundamentally interesting questions raised at the level of basic science, the phenomenon of amyloid formation has been a much studied topic using a large number of different experimental [10] and theoretical approaches [11,12]. Irrespective of the rationale for studying amyloid, the principal avenue of investigation has been the determination of amyloid reaction kinetics, with the ultimate goal being the complete elucidation of the nature of the reaction starting materials, kinetic pathway and end products along with a working understanding of how they are affected by changes in environmental conditions. By necessity the findings of such a kinetic based investigation must be expressed in terms of mathematical relations, which for a given set of conditions can reproduce the system behavior and additionally provide hypotheses for further experimental test. Despite the widespread nature of the investigative effort, as of the present day it would be fair to say that we have had limited success in the *de novo* prediction of the rate, extent or structural nature of the amyloid end product from an arbitrary polypeptide sequence in a chemically defined solution environment. Part of the barrier to achieving a detailed understanding of amyloid formation kinetics has been related to the relatively blunt experimental and theoretical tools that we have had at our disposal. Indeed for the last fifty years or so the principal methods for monitoring the kinetics of amyloid formation have been techniques, such as turbidity assay [13], dye binding [14] and filter binding [15], which yield a single experimental marker often taken as referring to the total mass of protein in aggregate form. Because of the sparse nature of the information available, statistical rate methods developed to interpret and analyze such experiments have themselves been constructed in terms of a single observable [16–20] and as such are somewhat limited in their ability to provide insight into the relationship between the size and shape of the amyloid distribution and the structural characteristics of the amyloid reaction starting and end products [3,21–24]. Following in the footsteps of Oosawa [25,26], traditional analytical models have been constructed in terms of averaged rate parameters describing nucleation rate constants, growth rate constants and a critical nucleus size. At the other extreme of the simulation spectrum, modern day particle based procedures utilizing molecular dynamics or Monte Carlo approaches have been used to examine the amyloid aggregation reaction [11,27–30]. These procedures are, in principle capable of providing pathway and structural information, however due to limitations in computing power they are as yet restricted to simulations involving small time scales and a small number (<100) of short peptides and therefore cannot be used for simulating or analyzing experimentally accessible regions of the amyloid reaction.

* Corresponding author. Fax: +81 29 853 8050.
E-mail address: damienhall@md.tsukuba.ac.jp (D. Hall).

0301-4622/$ – see front matter © 2008 Elsevier B.V. All rights reserved.
doi:10.1016/j.bpc.2008.11.013

In recent times increasingly sophisticated multi-experimental strategies [31–36] have provided detailed kinetic information on the evolution of the structure, distribution and total extent of all species within the aggregate population. In keeping with the greater density of available information a new modelling approach is required that is able to relate these diverse information strands and hence describe amyloid kinetics in greater detail. Here we present a general approach for the multi-scale simulation of the kinetics of the amyloid formation reaction that shows great potential for overcoming these problems and offers the potential to relate structural characteristics of the monomer and fibril, with the kinetic evolution of the amyloid distribution. The simulation approach combines both particle and statistical characteristics to first derive a set of rate constants which it then uses as parameters in a more traditional rate model of an amyloid polymerization reaction. The method outlined yields insight into how various properties of the polypeptide chain relate to kinetics of amyloid formation and the structure of the amyloid end product.

1. Theory

In this section we describe the theoretical model used to predict the rate constants for each step of the aggregation reaction and outline the procedure for incorporating these rate constants into a large scale simulation of amyloid formation.

1.1. Theoretical model for predicting amyloid reaction rate constants

In its simplest form [37] the rate constant, k_{ij}, for a bimolecular reaction between particles i and j can be treated as the product of a collision density term, ν_{ij} (M^{-1} s^{-1}), and a probability reflecting the successful outcome of the reaction P_{ij} (Eq. (1)).

$$k_{ij} = \nu_{ij} P_{ij} \tag{1}$$

We consider amyloid growth to occur by successive stepwise addition of monomer (making species i always refer to monomer ($i=1$)). Species j can range from a monomer to any higher order amyloid species, $1 \le j \le \infty$ with amyloid considered as any species $j \ge 2$. Here we use a modified version of the random flight model presented previously [38] to predict both P_{1j} and ν_{1j}. In this approach the molecular model of the unfolded polypeptide chain is set similar to that of a 3D random flight polymer—an approximation which allows for the derivation of a semi-analytical relationship for the particle model. As shown in Fig. 1 amyloid formation is considered to be driven by the intimate association of a number of key amino acids dispersed within a larger amyloidogenic peptide stretch with a corresponding identical stretch of amino acids located on a second polypeptide chain. For amyloid formation to occur each amyloidogenic stretch must adopt a defined conformation capable of participating in β-sheet formation upon contact with its binding partner. In this study the reaction potential is considered to be sufficiently energetically down hill such that the probability of success is dominated principally by configuration and orientation determinants. Using such an assumption we calculate the total probability, P_{1j}, of a successful interaction upon collision (Eq. (2a)) as the product of a set of conditional probabilities that each predict the likelihood of a certain event. We describe these individual probabilities for both monomer and amyloid ($j \ge 2$) for the following events (i.) P_u—the polypeptide is suitably unfolded (Eq. (2b), here we assume a simple two state model, K refers to the equilibrium unfolding constant and C_d the equilibrium concentration of denaturant and n the stoichiometry of the reaction), (ii.) P_c—the amyloidogenic peptide stretch is in the correct linear configuration (Eq. (2c)), (iii.) P_o—the major and minor axes lie within a cone with a set tolerance and that each of the individual key residues is correctly oriented with respect to its binding partner (three angular requirements) (Eq. (2d)) (iv.) P_{nf}—no frustration occurs from any additional non-amyloid forming peptide region at the N or C terminus (Eq. (2e)) (where P_{fN} and P_{fC} refer to the probability of frustration occurring at the N and C termini).

$$P_{1j} = \left[P_{1u} \cdot P_{ju}\right]\left[P_{1c} \cdot P_{jc}\right] \cdot \left[P_{1o} \cdot P_{jo}\right]\left[P_{1nf} \cdot P_{jnf}\right] \tag{2a}$$

$$P_{1u} = \frac{KC_d^n}{\left(1 + KC_d^n\right)};\ P_{ju} = 1 \tag{2b}$$

$$P_{1c} = P_1(r_{12})P_1(r_{23})P_1(r_{13} \pm \Delta r);\ P_{jc} = 1 \tag{2c}$$

$$P_{1o} = P_1(\phi)P_1(\psi)P_1(\theta);\ P_{jo} = P_1(\theta)(j=1);\ P_{jo} = 1(j>1) \tag{2d}$$

$$P_{1nf} = (1-P_{fN})(1-P_{fC});\ P_{jnf} = (1-P_{fN})(1-P_{fC})(j \ge 1) \tag{2e}$$

The collision density term is calculated based on knowledge of the diffusion constants for each interacting species, D_1 and D_j, and the cross section of radius, R_c, generated by the central amino acid residues of the amyloidogenic regions on each of the interacting partners. An approach of the two components was allowed to occur through the rounded face of a hemi-sphere proscribed by a radius of R_c which was made equal to 2 bond lengths of the random flight polymer chain approximant (in this case the average dimensions of one amino acid are such that $R_c = 16$ Å [39]). The translational diffusion constant for monomer (Eq. (3a)) was based on the diffusion of an equivalent sphere having a radius R equal to the root mean square radius of a Gaussian chain of (N) bond lengths where $N+1$ is the total number of amino acids in the unfolded protein [40]. For amyloid species of size $j \ge 20$ the translational diffusion constant was approximated using a relationship determined for the diffusion of a sphero-cylindrical rod of length $2a$ and radius b [41] shown by Eq. (3b). In this study each amyloid fibre was considered to grow from each end in a linear fashion. The centre of each peptide in an amyloid fibre was separated by a distance of R_c from its corresponding binding partner. To interpolate the translational diffusion coefficient for amyloid sizes $1 < j < 20$ a multi-exponential fit of the data set was made with the best fit parameters shown in Fig. 2. The collision density term was calculated on the basis of Eq. (3c), where N_A represents Avogadro's number.

$$D_1 = \frac{kT}{6\pi\eta R} \tag{3a}$$

$$D_j = \frac{kT}{6\pi\eta\left[\frac{(2/3)^{1/3}(a/b)^{2/3}}{\log_e(2a/b)-0.30}\right]\left(\frac{3b^2a}{2}\right)^{1/3}} \quad (j \ge 20) \tag{3b}$$

$$\nu_{1j} = 2\pi R_c (D_1 + D_j) N_A \qquad (\text{for } j \ge 1) \tag{3c}$$

1.2. Method for simulating large scale irreversible amyloid reactions

Amyloid growth was simulated using a modification of the stepwise polymerization model previously constructed to explicitly simulate microtubule polymerization kinetics [13,42]. In the present version of the model amyloid growth occurs irreversibly by addition of monomer, A_1, present at a concentration C_1, to any other species j of size ranging from 1 to N_{max}, present at a concentration C_j (Eq. (4)) [43]. The forward rate constants, k_{1j}, governing each stage of the amyloid formation process were calculated as described above.

$$A_j + A_1 \xrightarrow{k_{1j}} A_{j+1} \quad (\text{for } j \ge 1) \tag{4}$$

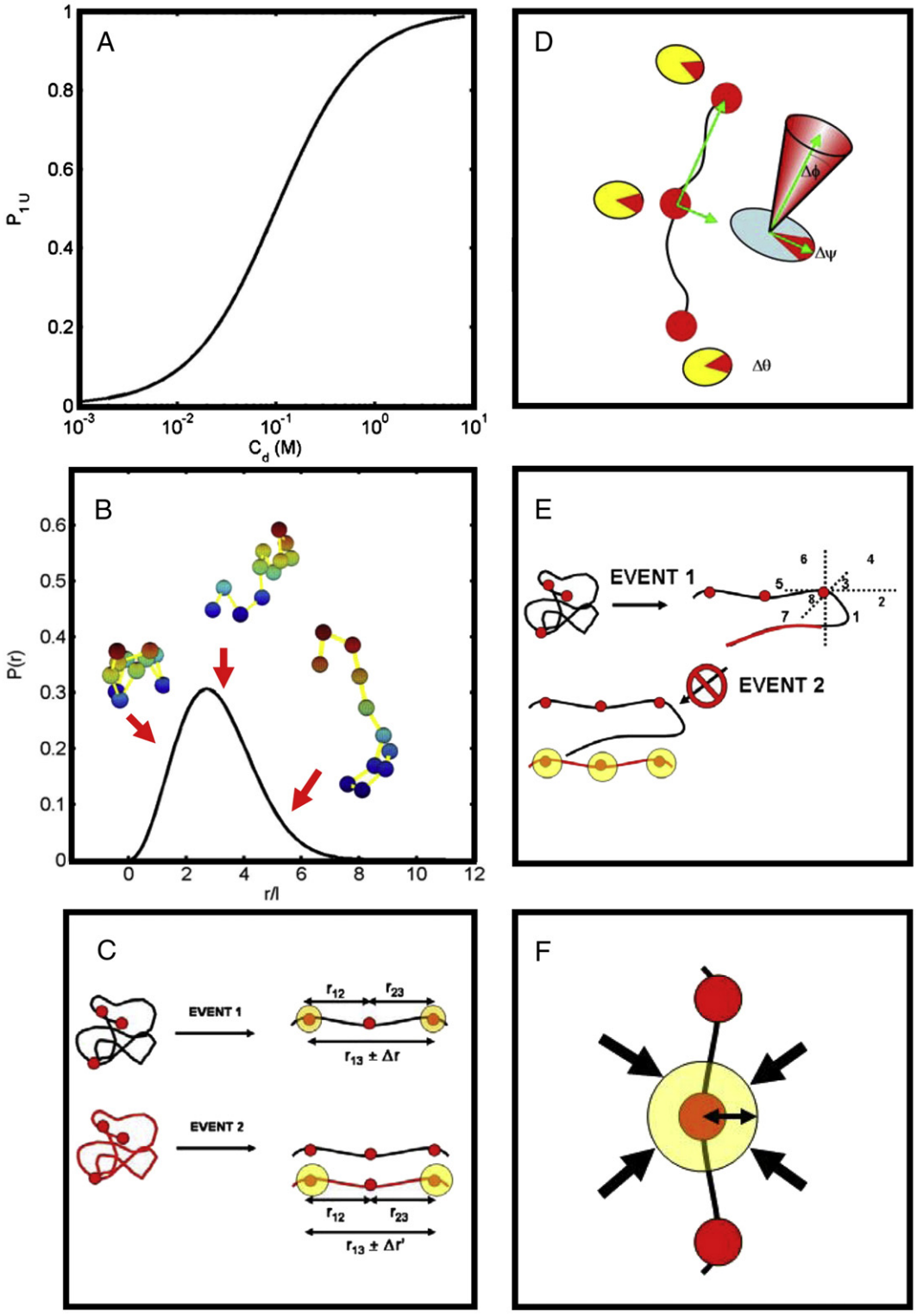

Fig. 1. Schematic describing the basic components of the particle model. (A) Unfolded Extent: The likelihood of the protein being unfolded is determined on the basis of a protein unfolding plot. (B) Polymer Statistics: A random flight statistical distribution, describing the range of end to end distances for a random flight polymer is used to estimate the likelihood of $P_1(r_{12})$ and $P_1(r_{23})$. (C) Configuration Probability: Each stepwise monomer addition event must satisfy two configuration requirements, *event 1* requires the first peptide to adopt a certain set of internal co-ordinates (defined by distances r_{12}, r_{23} and $r_{13} \pm \Delta r$ between three key residues shown in red), *event 2* requires that the second peptide adopts a less stringent set of internal co-ordinates (defined by distances r_{12}, r_{23} and $r_{13} \pm \Delta r'$ between three key residues). (D) Orientation Probability: Upon encounter a monomer must be correctly oriented with respect to its interacting partner. One member of the interacting pair must satisfy three angular requirements (ϕ,θ,ψ), the other member must satisfy only one angular requirement (θ). (E) Frustration Probability: The model accounts for the possibility of frustration by an adjacent segment of non-amyloid forming polypeptide chain. (F) Collision Frequency: The rate of collisions between interacting species was determined on the basis of a collision cross-section type argument based on the rate of each particles' diffusion through solution and subsequent encounter about the designated central residue. (For interpretation of the references to color in this figure legend, the reader is referred to the web version of this article.)

The set of interrelated first order differential equations denoting the rate of change of the concentration of species of degree $j+1$, (dC_{j+1}/dt) (Eq. (5)) was solved using a numerical integration strategy [42] capable of coping with large and stiff sets of differential equations.

$$dC_{j+1}/dt = k_{1j}C_jC_1 - k_{1(j+1)}C_{j+1}C_1 \quad (\text{for } j \geq 2) \tag{5}$$

A total of up to 10,000 inter-related rate equations were considered in a single simulation although this number was allowed to grow as required so as to allow for rapid solution of the set of rate equations.

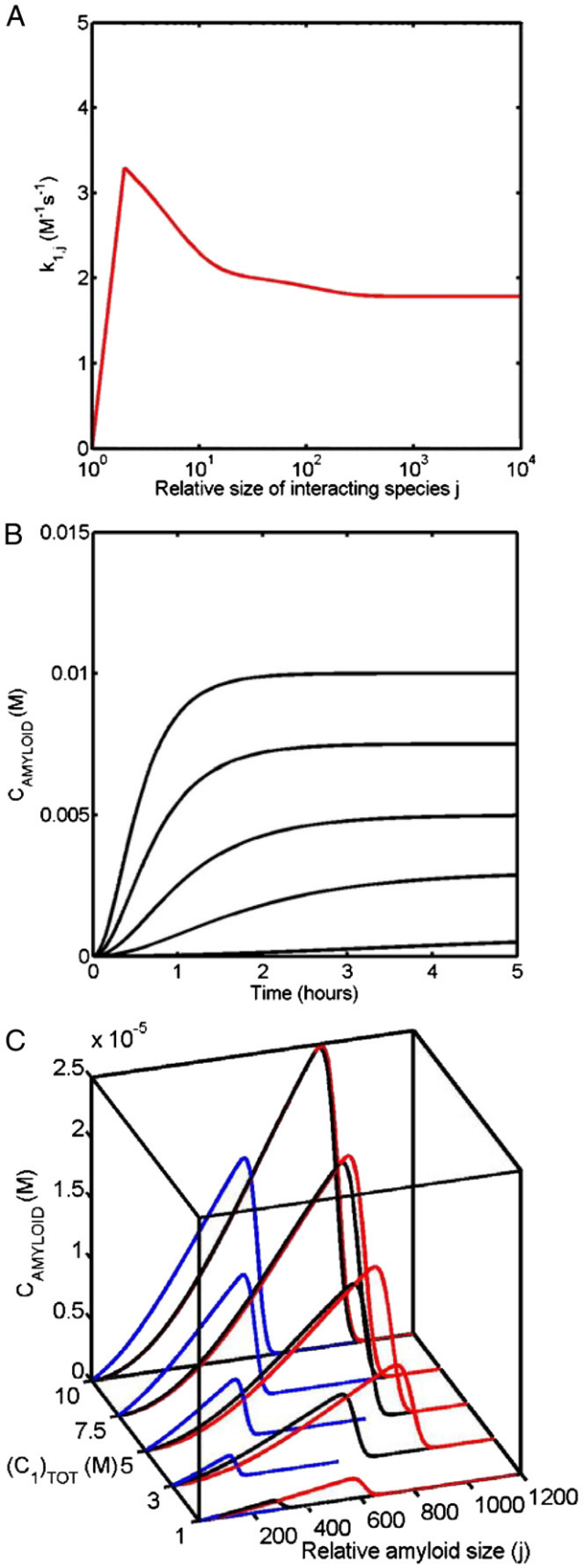

Fig. 2. Multi-scale simulation exploring the effect of concentration on the kinetics of formation of amyloid by an 11 amino acid peptide: (A) Structure and size specific rate constants, k_{1j}, calculated using the particle based collision reaction model. The value of k_{11} is 5.6×10^{-6} M^{-1} s^{-1}. (B) Rate of amyloid formation (weight concentration of all amyloid species) at 5 different starting concentrations of monomer (10, 7.5, 5, 3 and 1 mM) from top to bottom respectively. (C) Time dependence of the evolution of the amyloid length distribution for the five different starting concentrations of monomer. The first second and third (blue, black and red respectively) lines refer to 'snapshots' taken at 0.5, 2 and 5 h respectively. The time displayed represents 'real time' in the sense that this would be the time taken by an amyloid formation reaction governed by the specific rate constants calculated from the particle model geometry (as a function of the particular conformation and orientation requirements). (For interpretation of the references to color in this figure legend, the reader is referred to the web version of this article.)

2. Results

We consider two tests of the multi-scale simulation approach on an 11 amino-acid polypeptide that is known from prior information to have a strong tendency to form amyloid. Test case A is concerned with the effect of variation in the initial starting concentration of this highly amyloidogenic peptide. Test case B examines the effect of the presence of different lengths of a non-amyloidogenic flanking region attached to the end of the amyloidogenic peptide where the non-amyloidogenicity of the flanking region was inferred from prior information. In both cases we first use the particle model of the amyloid formation reaction to calculate the rate constants for each individual bimolecular reaction. Next we incorporate the calculated rate constants into the polymer kinetic routine to calculate the nature of the amyloid mass formation and size distribution kinetics.

2.1. Effect of concentration

Fig. 2 describes the case of amyloid formation from an 11 amino acid peptide over a 10 fold concentration range. The particle model rate constant calculation (Fig. 2A) reveals an effective nucleation rate barrier at the stage of dimer formation. The solution of the large set of differential equations shown by Eq. (5), with the calculated rate constants included as parameters, reveals a sigmoidal kinetic pattern (Fig. 2B)—a phenomenon that is characteristic of nearly all amyloid formation reactions. The effects of concentration can be noted on both the kinetics of total amyloid mass concentration formation (Fig. 2B) and the evolution of the amyloid polymer distribution (Fig. 2C).

2.2. Effect of overhanging peptide sequence

In this test case we examine the differences between amyloid formation from an 11 amino acid amyloidogenic peptide having different lengths of overhanging polypeptide sequence at one of the peptide termini (see Fig. 1E). The overhanging polypeptide regions were considered to vary in length from 0 to 50 amino acids in 10 amino acid increments. All simulations were performed at the starting concentration of 10 mM polypeptide in monomeric form. Fig. 3A describes the three dimensional surface generated by the particle model rate constant calculation for the differently sized species and the different lengths of polypeptide overhang. We note that the particle model predicts that the effect of the polypeptide overhang will be to frustrate the chance of a successful collision and to hence decrease the value of the rate constant. This decrease in the calculated value of the rate constants translated into

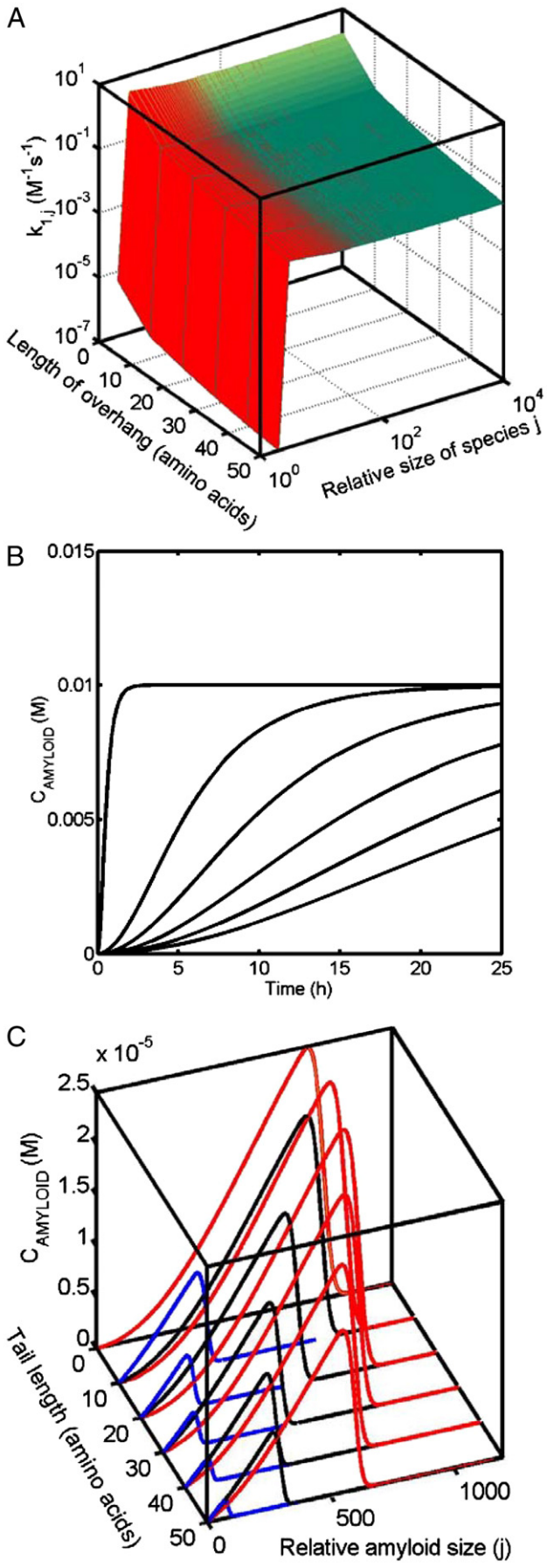

a marked slowing of the amyloid growth kinetics at both the level of total amyloid mass (Fig. 3B) and the evolution of the size distribution (Fig. 3C).

3. Discussion

With more experimental information provided by modern techniques, more sophisticated simulation and analysis methods are required to properly integrate the available experimental data. Other researchers have also turned their eyes toward more detailed modelling strategies, of particular note is the work by Pallitto and Murphy [44] and Carrotta et al. [45]. What makes our approach distinct is that our model can semi-quantitatively incorporate diverse information streams concerning monomer structure, amyloid internal structure, amyloid external structural information (relating to the amyloid size distribution) and the total mass fraction of amyloid formed. Here we have used our model to simulate the kinetics of amyloid formation from a specific conformational state of an unstructured polypeptide using a set of theory derived rate constants as parameters in a large scale polymerization simulation. The use of a three point internal structural designation allows us to include a conformation specific requirement within the amyloidogenic region of the monomer. Likewise the allowance for structural frustration means that for the first time we may begin to semi-quantitatively examine sequence position effects [46]. As such our simulation approach combines elements of both structural particle based simulations with more traditional statistical rate approaches to access experimentally relevant time and size domains. To demonstrate our multi-scaling approach we approximated the unfolded polypeptide (which constitutes the monomeric building block of the amyloid fibril) as a random flight polymer chain. The important point to note is that we are using a polymer model for which a governing probability distribution exists. Such a correspondence could be similarly generated by the use of experimentally obtained distribution information as might be generated from NMR, FRET or hydrodynamic measurements.

Perhaps the most striking feature of the current work was the finding that the characteristic sigmoidal kinetic pattern typically associated with amyloid reactions [1,6,12,17,18,20,31] was generated as a natural consequence of our model rather than from an arbitrary choice of rate parameters. In the classical helical polymerization theory of Oosawa et al. [25,26] nucleation is usually thought of as being defined on potential energetic/structural grounds, typically associated with helix formation, and indeed nearly all kinetic models used to describe polymerization reactions associated with microtubule and microfilament formation have been rationalized in these terms [47–49]. However in our model the nucleation step is generated by the configuration entropy of the unfolded polypeptide chain, i.e. the inherently lower probability that two unfolded chains will both be in the necessary conformation upon meeting. Furthermore the current work has indicated that a non-amyloid forming adjacent unstructured polypeptide region may dramatically slow the rate of amyloid formation from an amyloidogenic peptide due to the potential for frustration of the collision event.

To demonstrate the current multi-scale approach we have limited ourselves to the simplest 1D reaction model, that of endwise irreversible monomer addition. However the model is capable of further refinement for use in both simulation and analyses of data, principally by factoring

Fig. 3. Multi-scale simulation exploring the effect of increasing the length of an 'overhanging tail region' of non-amyloidogenic peptide present at a single end of the amyloidogenic 11 residue polypeptide on the kinetics of amyloid formation. (A) Structure and size specific rate constants, k_{1j}, calculated using the particle based collision reaction model. Frustration by the overhanging tail was calculated by computing the likelihood that any region of the tail interrupted a successful collision (see Fig. 1E). (B) Rate of amyloid formation (weight concentration of all amyloid species) affected by 6 different lengths of overhanging tail (all at an initial starting concentration of monomer of 10 mM). (C) Time dependence of the evolution of the amyloid length distribution for the six different lengths of tail. First, second and third (blue, black and red respectively) lines refer to 'snapshots' taken at 2.5, 10 and 25 h respectively. (For interpretation of the references to color in this figure legend, the reader is referred to the web version of this article.)

in the concept of reversibility. To be certain our dynamic based approach is not the only method for attempting the multi-scale simulation of the amyloid kinetic reaction. A master equation type approach based on the definition of a potential energy landscape can achieve a similar scaling effect [50]. In this approach a multi-dimensional matrix of pathway connected regions of the reaction coordinate potential energy surface is first constructed using a Monte-Carlo search strategy. The transition rate between neighbouring regions in the matrix is then calculated using a form of transition state reaction rate theory. Although such an approach has greater potential than the simplified dynamic approach outlined here a number of outstanding issues relating to reaction coordinate connectivity between neighboring regions and the full enumeration of the reaction coordinate potential energy landscape make its application to protein aggregation still a work in progress at the current time. With these caveats clearly stated we believe that our approach represents the basic framework for a multi-scale simulation strategy that can relate structural information concerning the monomer and amyloid to kinetic observables and in doing so can begin to advance the state of simulation and analysis of amyloid aggregation kinetics from the techniques developed by Oosawa approximately 50 years ago.

Acknowledgements

This research was supported in part by the Japanese Science and Technology Agency (JST) and the University of Tsukuba under the special coordinated scheme 'Funds in Aid of the Promotion of Young Scientists' Independent Research.' We would like to thank Dr. Reed Wickner for providing useful comments on an early draft of this manuscript.

Appendix A

Details of the model

In this section we provide details relating to the nature of the 'particle' model, the equations used to represent it and the parameters used in this paper. The amyloidogenic region was considered as an 11 node Gaussian chain. Three residues located at the centre and two ends of the chain were used to define a basic structure. In calculating the configuration probabilities $P_1(r_{12})$ and $P_1(r_{23})$ the standard equation for a 3D Gaussian chain was used (Eq. (A1)).

$$P_1(r_{12}) = 4\pi\left(\frac{3}{2\pi(N_{12})L^2}\right)^{3/2}(\kappa N_{12})^2 e^{\left(\frac{-3(\kappa N_{12})^2}{2N_{12}L^2}\right)} \tag{A1}$$

Here N_{12} represents the number of bond lengths in the chain length considered ($N_{12}=5$ for the current case for the chain segment r_{12}), L is the chain bond length (here set to 1) and κ is a scaling variable set from 0 to 1 to define the length of the 6 node chain in relation to its maximum length of 5 bond lengths. On the condition that both segments r_{12} and r_{23} were at their required lengths the probability that the end to end distance r_{13} was at a set length (plus or minus a given tolerance) was calculated by treating the system as a virtual 3 node chain (Eq. (A2)). The required distance, r_{13}, was denoted by the scaling factor ε and the total number of bond lengths N_{13} in the 11 node segment. An error tolerance of $\Delta(\varepsilon N_{13})$ was allowed. If $\varepsilon N_{13}+\Delta(\varepsilon N_{13})$ exceeded the physical maximum then N_{13} was chosen instead as the leading integration limit. Likewise unphysical negative distances were replaced by zero.

$$P_1(r_{13}) = \left[\frac{-\cos\lambda}{2}\right]_{\lambda=\cos^{-1}\left[1-\frac{(\varepsilon N_{13}+\Delta(\varepsilon N_{13}))^2}{2(\kappa N_{12})^2}\right]}^{\lambda=\cos^{-1}\left[1-\frac{(\varepsilon N_{13}-\Delta(\varepsilon N_{13}))^2}{2(\kappa N_{12})^2}\right]} \tag{A2}$$

In this paper we considered the adoption of a unique structure as the starting prerequisite for amyloid formation. The end peptide of an already formed amyloid fibril was considered as fulfilling this structural requirement ($P_{j\_c}=1$). At the nucleation level we considered that at least one of the interacting monomers must adopt the required structure to a high degree of tolerance ($\Delta(\varepsilon N_{13})\rightarrow 0$). For both the nucleating and elongation events the second participating monomer was allowed to have a greater associated structural error ($\Delta(\varepsilon N_{13})>0$). On the condition that the two central residues had collided in the correct configuration, the orientation probability, P_{1_O} (Eq. (2d)) was calculated on the basis of three angular requirements (Eqs. (A3a), (A3b) and (A3c)). First that the axis defined by the line segment r_{12} lays in a cone with a set tolerance given by $\Delta\phi$ (here set equal to $\pi/2$), the second that each of the individual key residues was correctly oriented with respect to its binding partner (here $\Delta\theta=\pi$) and the third that the component of the vector traced by the line r_{23} that is normal to the axis defined by r_{12} lies within the segment $\Delta\psi$ (here set equal to $\pi/2$). In the present work ε was set at 0.7 and κ was set at 0.4 making the structure effectively linear.

$$P_1(\phi) = \left[\frac{-\cos\phi}{2}\right]_0^{\Delta\phi} \tag{A3a}$$

$$P_1(\theta) = \left\{\left[\frac{\theta}{2\pi}\right]_0^{\Delta\theta}\right\}^3 \tag{A3b}$$

$$P_1(\psi) = \left[\frac{\psi}{2\pi}\right]_0^{\Delta\psi} \tag{A3c}$$

The likelihood of frustration caused by an overhanging tail segment was calculated by computing the probability that any section of the random flight tail region existed in the two quadrants in which the association between the two amyloidogenic peptides took place. This probability was determined by collating the results of 500 repeated trials of a random walk (for each overhanging tail length) for tail lengths from 10 to 50 amino acids. The results were fitted to an empirical expression and the results of this fitting procedure are shown in Eq. (A4).

$$P_f = 0.275\left[1-e^{-0.041N}\right] + 0.551\left[1-e^{0.492N}\right] \tag{A4}$$

References

[1] J.D. Sipe, A.S. Cohen, Review: history of the amyloid fibril, J. Struct. Biol. 130 (2000) 88–98.
[2] U. Baxa, Structural basis of infectious and non-infectious amyloids, Curr. Alzheimer Res. 5 (2008) 308–318.
[3] O. Sumner Makin, L.C. Serpell, Structures for amyloid fibrils, FEBS J. 272 (2005) 5950–5961.
[4] E.D. Ross, A.P. Minton, R.B. Wickner, Prion domains: sequences, structures and interactions, Nat. Cell Biol. 7 (2005) 1039–1044.
[5] K.J. Binger, C.L. Pham, L.M. Wilson, M.F. Bailey, L.J. Lawrence, P. Schuck, G.J. Howlett, Apolipoprotein C-II amyloid fibrils assemble via a reversible pathway that includes fibril breaking and rejoining, J. Mol. Biol. 376 (2008) 1116–1129.
[6] M. Stefani, C.M. Dobson, Protein aggregation and aggregate toxicity: new insights into protein folding, misfolding diseases and biological evolution, J. Mol. Med. 81 (2003) 678–699.
[7] M.B. Pepys, Amyloidosis, Annu. Rev. Med. 57 (2006) 223–241.
[8] M.M. Barnhart, M.R. Chapman, Curli biogenesis and function, Annu. Rev. Microbiol. 60 (2006) 131–147.
[9] E. Gazitm, Self-assembled peptide nanostructures: the design of molecular building blocks and their technological utilization, Chem. Soc. Rev. 36 (2007) 1263–1269.
[10] I.W. Hamley, Peptide fibrillization, Angew. Chem. Int. Ed. 46 (2007) 8128–8147.
[11] B. Ma, R. Nussinov, Simulations as analytical tools to understand protein aggregation and predict amyloid conformation, Curr. Opin. Chem. Biol. 10 (2006) 445–452.
[12] R.M. Murphy, Kinetics of amyloid formation and membrane interaction with amyloidogenic proteins, Biochim. Biophys. Acta. 1768 (2007) 1923–1934.
[13] D. Hall, A.P. Minton, Turbidity as a probe of tubulin polymerization kinetics: a theoretical and experimental re-examination, Anal. Biochem. 345 (2005) 198–213.
[14] H. Levine III, Quantification of β-sheet amyloid fibril structures with thioflavin T, Meth. Enzymol. 309 (1999) 274–284.
[15] E. Wanker, E. Scherzinger, V. Heiser, A. Sittler, H. Eickhof, H. Lehrach, Membrane filter assay for detection of amyloid like polyglutamine containing protein aggregates, Meth. Enzymol. 309 (1999) 375–385.

[16] J.L. Larson, A.D. Miranker, The mechanism of insulin action on islet amyloid polypeptide fiber formation, J. Mol. Biol. 335 (2004) 221–231.
[17] A.M. Morris, M.A. Watzky, J.N. Agar, R.G. Finke, Fitting neurological protein aggregation kinetic data via a 2-step, minimal/'Ockham's Razor' model: the Finke-Watzky mechanism of nucleation followed by autocatalytic surface growth, Biochemistry 47 (2008) 2413–2427.
[18] J. Masel, V.A. Jansen, M.A. Nowak, Quantifying the kinetic parameters of prion replication, Biophys. Chem. 77 (1999) 139–152.
[19] M. Colaco, J. Park, H. Blanch, The kinetics of aggregation of poly-glutamic acid based polypeptides, Biophys. Chem. 136 (2008) 74–86.
[20] S. Chen, F.A. Ferrone, R. Wetzel, Huntington's disease age-of-onset linked to polyglutamine aggregation nucleation, Proc. Natl. Acad. Sci. U. S. A. 99 (2002) 11884–11889.
[21] N. Ferguson, J. Becker, H. Tidow, S. Tremmel, T.D. Sharpe, G. Krause, J. Flinders, M. Petrovich, J. Berriman, H. Oschkinat, A.R. Fersht, General structural motifs of amyloid protofilaments, Proc. Natl. Acad. Sci. U. S. A. 103 (2006) 16248–16253.
[22] R. Tycko, Molecular structure of amyloid fibrils: insights from solid-state NMR, Q. Rev. Biophys. 39 (2006) 1–55.
[23] T.D. Ding, J.D. Harper, Analysis of amyloid-β assemblies using tapping mode atomic force microscopy under ambient conditions, Meth. Enzymol. 309 (1999) 510–525.
[24] L.C. Serpell, SmithJ.M. , Direct visualisation of the β-sheet structure of synthetic Alzheimer's amyloid, J. Mol. Biol. 299 (2000) 225–231.
[25] F. Oosawa, M. Kasai, Theory of linear and helical aggregations of macromolecules, J. Mol. Biol. 4 (1962) 10–21.
[26] F. Oosawa, S. Asakura, Thermodynamics of the Polymerization of Protein, Academic Press, New York, 1975.
[27] M.T. Oakely, J.M. Garibaldi, J.D. Hirst, Lattice models of peptide aggregation: evaluation of conformational search algorithms, J. Comput. Chem. 26 (2005) 1638–1646.
[28] D.M. Standley, Y. Yonezawa, Y. Goto, H. Nakamura, Flexible docking of an amyloid-forming peptide from beta(2)-microglobulin, FEBS Lett. 580 (2006) 6199–6205.
[29] O. Zimmermann, U.H. Hansmann, Understanding protein folding: small proteins in silico, Biochim. Biophys. Acta. 1784 (2008) 252–258.
[30] B. Urbanc, L. Cruz, D.B. Teplow, H.E. Stanley, Computer simulations of Alzheimer's amyloid beta-protein folding and assembly, Curr. Alzheimer Res. 3 (2008) 493–504.
[31] A. Lomakin, G.B. Benedek, D.B. Teplow, Monitoring protein assembly using quasielastic light scattering spectroscopy, Meth. Enzymol. 309 (1999) 429–459.
[32] A.J. Baldwin, S.J. Anthony-Cahill, T.P. Knowles, G. Lippens, J. Christodoulou, P.D. Barker, C.M. Dobson, Measurement of amyloid fibril length distributions by inclusion of rotational motion in solution NMR diffusion measurements, Angew. Chem. Int. Ed. 47 (2008) 3385–3387.
[33] T. Chiba, Y. Hagihara, T. Higurashi, K. Hasegawa, H. Naiki, Y. Goto, Amyloid fibril formation in the context of full-length protein: effects of proline mutations on the amyloid fibril formation of beta2-microglobulin, J. Biol. Chem. 278 (2003) 47016–47024.
[34] W. Qi, A. Zhang, D. Patel, S. Lee, J.L. Harrington, L. Zhao, D. Schaefer, T.A. Good, E.J. Fernandez, Simultaneous monitoring of peptide aggregate distributions, structure, and kinetics using amide hydrogen exchange: application to Abeta(1-40) fibrillogenesis, Biotechnol. Bioeng. 100 (2008) 1214–1227.
[35] S.N. Bagriantsev, V.V. Kushnirov, S.W. Liebman, Analysis of amyloid aggregates using agarose gel electrophoresis, Meth. Enzymol. 412 (2006) 33–48.
[36] D.C. Thorn, H. Ecroyd, M. Sunde, S. Poon, J.A. Carver, Amyloid fibril formation by bovine milk αs2-casein occurs under physiological conditions yet is prevented by its natural counterpart, αs1-casein, Biochemistry 47 (2008) 3926–3936.
[37] K.J. Laidler, Chemical Kinetics, 2nd ed.Harper and Row, New York, 1987.
[38] D. Hall, N. Hirota, C.M. Dobson, A toy model for predicting the rate of amyloid formation from unfolded protein, J. Mol. Biol. 351 (2005) 195–205.
[39] M. Lund, B. Jönsson, A mesoscopic model for protein–protein interactions in solution, Biophys. J. 85 (2003) 2940–2947.
[40] C.R. Cantor, P.R. Schimmel, Biophys. Chem. (1980) 979–1018 Part 3. Ch. 18.
[41] V. Bloomfield, W.O. Dalton, K.E. van Holde, Frictional coefficients of multisubunit structures. I. Theory, Biopolymers 5 (1967) 135–148.
[42] D. Hall, The effects of Tubulin denaturation on the characterization of its polymerization behaviour, Biophys. Chem. 104 (2003) 655–682.
[43] S.R. Collins, A. Douglass, R.D. Vale, J.S. Weissman, Mechanism of prion propagation: amyloid growth occurs by monomer addition, PLOS 2 (2004) 1582–1590.
[44] M.M. Pallitto, R.M. Murphy, A mathematical model of the kinetics of beta-amyloid fibril growth from the denatured state, Biophys. J. 81 (2001) 1805–1822.
[45] R. Carrotta, M. Manno, D. Bulone, V. Martorana, P.L. San Biagio, Protofibril formation of amyloid beta-protein at low pH via a non-cooperative elongation mechanism, J. Biol. Chem. 280 (2005) 30001–30008.
[46] D.C. Masison, R.B. Wickner, Prion-inducing domain of yeast Ure2p and protease resistance of Ure2p in prion-containing cells, Science 270 (1995) 93–95.
[47] W.A. Voter, H.P. Erickson, The kinetics of microtubule assembly. Evidence for a two-stage nucleation mechanism, J. Biol. Chem. 259 (1984) 10430–10438.
[48] Y. Engelborghs, L.C. De Maeyer, N. Overbergh, A kinetic analysis of the assembly of microtubules in vitro, FEBS Lett. 80 (1977) 81–85.
[49] A. Wegner, J. Engel, Kinetics of the cooperative association of actin to actin filaments, Biophys. Chem. 3 (1977) 215–225.
[50] J. Lu, C. Zhang, R. Stephen Berry, Kinetics of model energy landscapes: an approach to complex systems, Phys. Chem. Chem. Phys. 7 (2005) 3443–3456.